Available online at www.sciencedirect.com

SCIENCE DIRECT®

Journal of Molecular Catalysis A: Chemical 198 (2003) 263–275

JOURNAL OF MOLECULAR CATALYSIS A: CHEMICAL

www.elsevier.com/locate/molcata

CO_2 reforming of CH_4 over Ru/zeolite catalysts modified with Ti

S.M. Gheno [a], S. Damyanova [b], B.A. Riguetto [c], C.M.P. Marques [c], C.A.P. Leite [a], J.M.C. Bueno [a,*]

[a] *DEQ-Universidade Federal de São Carlos, Caixa Postal 676, 13565-905 Sao Carlos, SP, Brazil*
[b] *Institute of Catalysis, Bulgarian Academy of Sciences, 1113 Sofia, Bulgaria*
[c] *DQ-Universidade Federal de São Carlos, Caixa Postal 676, 13565-905 Sao Carlos, SP, Brazil*

Received 16 September 2002; accepted 3 December 2002

Abstract

Ru/NaY and Ru/USY catalysts were prepared by ion exchange from an aqueous solution of $[Ru(NH_3)_6]Cl_3$. The effect of titanium on the structure of Ru/zeolite introduced by ion exchange or impregnation method from aqueous solution of $(NH_4)_2TiO(C_2O_4)_2{\cdot}H_2O$ was investigated. The samples were characterized by different techniques, using X-ray diffraction (XRD), UV-Vis diffuse reflectance spectroscopy (DRS), temperature-programmed desorption of hydrogen (TPD-H_2), Fourier transform infrared spectroscopy (FTIR) of CO adsorption and transmission electron microscopy (TEM). Introduction of titanium into Ru/NaY zeolite by ion exchange caused a significant structural collapse of the zeolite framework. Contrary to that, TEM data showed that Ti incorporated into Ru/USY by ion exchange was well distributed within the zeolite cavities. The crystallinity of the USY zeolite decreased significantly after introduction of Ti by impregnation method and a separate phase of titania was formed. The effect of Ti content on the catalytic behavior of zeolite-supported Ru catalysts in the reaction of CO_2 reforming of CH_4 was elucidated. The higher specific activity of Ti-containing catalysts related to CO formation was caused by the both factors, the acceleration of CH_xO decomposition (precursor for CO formation) on metal-support interface and participation of the reverse of water gas shift reaction.

Keywords: Zeolite-supported Ru catalysts; USY; NaY; Titania; CO_2 reforming of CH_4

1. Introduction

During the last decade the catalytic reforming of methane with carbon dioxide has increasing interest as an alternative route for syngas production [1]. This process is attractive industrially due to low H_2/CO product ratio, which is preferable for Fisher–Tropsch synthesis processes [2]. The high reaction enthalpies associated with methane reforming by carbon dioxide and its reverse reaction make this process one of the most suitable for application in the storage of renewable energy sources [3]. Natural gas reforming is questionable as to whether CH_4/CO_2 reforming can contribute to a solution of greenhouse problems. Reducing of sources of CH_4 and non-CO_2 greenhouse gases could lead to a decline in the rate of the global warming, reducing the danger of dramatic climate change [4]. However, transformation of CH_4 and CO_2 into synthesis gas followed by subsequent conversion via Fisher–Tropsh synthesis into fuels that would be sources for CO_2 emissions.

Considerable effort has been made towards the design and development of active, selective and stable

* Corresponding author.
E-mail address: jmcb@power.ufscar.br (J.M.C. Bueno).

1381-1169/02/$ – see front matter © 2002 Elsevier Science B.V. All rights reserved.
doi:10.1016/S1381-1169(02)00695-7

catalyst for the reforming reaction of methane with carbon dioxide. The study of the catalysts for this reaction has been mainly focused on: (i) the dispersion and specific activity of metal phase; (ii) the stability towards carbon deposition; and (iii) the type of the support most suitable for improving the efficiency of the catalyst and the reaction mechanism. Industrially, the metal of choice for the catalyst is nickel supported on different carriers [5–7], due to its inherent availability and lower cost in comparison with noble metals. However, because the high endothermicity of the reaction, which requires high reaction temperature, supported nickel catalysts are more susceptible to coking than noble metals [8,9].

It has been shown, that specific noble metal may exibit different activity, depending on the nature of support. In several studies Ru and Rh supported on different oxides supports, like TiO_2 [1–12], MgO [11], Al_2O_3 [9–16] or silica [16], have shown a superior activity in the reaction of CO_2 reforming of methane. However the thermal stability of these catalysts has been very low. It is interesting to note that when the noble metals are supported on zeolite present extremely high thermal stability independently on the method of preparation [17,18]. These behaviors of the catalysts have been interpreted in terms of the structure sensitivity of the reaction and/or by participation of the support in the activation of methane and carbon dioxide molecules by introducing of an electron donation to the lowest unoccupied anti-bonding molecular orbital [9].

It is well known that TiO_2 is one of the most widely used transition metal oxides in catalysis. On the other hand, a dispersion of titania in microporous zeolite of high surface area would be effective to increase the number of surface active sites of TiO_2. In previously our work [10] we have observed that when Ru was supported on TiO_2 exhibited very high activity in CO_2 reforming of CH_4 compared to that for Ru supported on NaY zeolite, followed by a rapid deactivation. Therefore, it would be very important to combine ruthenium with titania to obtain a catalyst with optimal catalytic properties, combining the unique stability of zeolite-supported Ru catalyst with the high activity of titania-supported Ru [10].

To our knowledge, our work is the first attempt to investigate the effect of titanium introduced by different methods on the structure and catalytic behavior of Ru-containing zeolite NaY and USY catalysts in the reaction of CH_4 reforming with CO_2. The work was concentrated on: (i) the effect of the type of zeolite support on the morphology of metal components; (ii) the method of introducing of Ti; and (iii) the influence of Ti content. Different techniques were applied for characterization of the samples: X-ray diffraction (XRD), UV-Vis diffuse reflectance spectroscopy (DRS), temperature-programmed desorption of hydrogen (TPD-H_2), Fourier transform infrared spectroscopy (FTIR) and transmission electron microscopy (TEM).

2. Experimental

2.1. Preparation of samples

NaY zeolite support was prepared from LZ Y-54 (Si/Al = 2.6, Linde Molecular Sieves, Lot No. UOP-35-709). To remove the extra framework aluminium the HUSY zeolite from EZ-190P (Engelhard) was treated with an aqueous solution of H_2SO_4 at pH 4.5 and temperature of 343 K, accompanied with a significant increasing of Si/Al ratio from 5.66 to 10.14 (Table 1). For obtaining of NH_4USY zeolite the HUSY zeolite was treated by two successive exchanges with a solution of NH_4NO_3 ($3\,mol\,l^{-1}$) for 24 h at room temperature. After that the sample was keep in desiccator with NH_4Cl. Ruthenium was encapsulated into the NaY and NH_4USY supports by ion exchange using aqueous solution of $[Ru(NH_3)_6]Cl_3$ (Strem Chemicals, −99%). The ion-exchange procedure involved slowly adding of the dilute solution of $[Ru(NH_3)_6]Cl_3$ ($0.045\,g\,l^{-1}$) to a rapidly stirred zeolite slurry at room temperature over a period of 24 h. The Ru-exchanged NaY and USY zeolite samples were washed with deionized water until Cl^- detection with Ag^+ was negative. The samples were dried under vacuum at room temperature. The Ru/zeolite catalysts were carried out in a helium flow (UHP-5.0, AGA-Brasil) of $100\,ml\,min^{-1}$ at $2\,K\,min^{-1}$ from room temperature up to 773 K, the held at the respective temperature for 30 min. Heating in helium was necessary to avoid the formation of volatile RuO_4. The theoretical amount of Ru was about 3 wt.%.

Titanium-exchanged Ru/zeolites were prepared via ion exchange with an aqueous solution of ammonium

Table 1
Chemical analysis and structural properties for Ru and RuTi/zeolite catalysts

Sample	Ru (wt.%)	Ti (wt.%)	Ru/Al (bulk)	Ti/Al (bulk)	Si/Al (bulk)	Si/Al (XRD)	a_0	N_{Al}/cu
NaY	–	–	–	–	2.60	2.61	24.65	53.24
Ru/NaY	2.91	–	0.08	–	2.75	2.74	24.63	51.26
RuTi/NaY	2.88	3.03	0.29	0.64	12.67	8.51	24.36	20.18
HUSY	–	–	–	–	5.66	10.61	24.37	16.53
NH_4USY	–	–	–	–	10.14	10.65	24.36	16.48
Ru/USY	2.15	–	0.18	–	10.71	10.61	24.37	16.52
RuTi/USY	2.13	2.05	0.19	0.39	11.73	10.74	24.36	16.38
Ru(2)Ti_i/USY	1.86	1.95	0.17	0.37	11.54	10.66	24.36	16.45
Ru(4)Ti_i/USY	1.72	4.02	0.17	0.78	11.96	10.46	24.36	16.75

titanyl oxalate monohydrate, $(NH_4)_2TiO(C_2O_4)_2{\cdot}H_2O$ (Aldrich, 99.99% purity) (ATO), similar to the procedure reported by Liu et al. [19,20]. The ATO salt was chosen because the task was to find a titanium salt, which is soluble in water and toes not form colloidal suspensions. Ti-containing samples were filtered, washed with deionized water and dried under vacuum. The theoretical amount of ion exchanged Ti was 3 wt.%. The samples were abbreviated as RuTi/NaY and RuTi/USY. Other samples were prepared by impregnation of Ru/USY zeolite with an aqueous solution of $(NH_4)_2TiO(C_2O_4)_2{\cdot}H_2O$. In order to increase the amount of Ti the impregnation procedure was repeated. Ti-containing zeolites were dried and calcined by the same procedure cited above. The Ru content was 2 wt.% in Ti-impregnated samples. The samples were abbreviated as Ru(x)Ti_i/USY, where x is the theoretical amount of Ti (2 and 4 wt.%). The Ti content of the samples determined by ICP is listed in Table 1.

2.2. Methods

Chemical composition of the prepared samples (Si, Al, Ru, Ti) was determined by inductively coupled plasma-atomic emission spectrometry (ICP) for the samples dissolved in H_2SO_4:HF (1:1) solutions. The composition of the samples is listed in Table 1.

XRD patterns were carried out by a Rigaku–Denki diffractometer using Cu Kα radiation (50 kV, 100 mA) with a Ni filter. The step-scans taken over the range of 2θ from 3 to75 in step of 0.020°, the intensity data for each is being collected for 5 s. Unit cell parameters (a_0), the number of Al per unit cell, N_{Al}/cu, and Si/Al ratios were calculated accordingly [21]. The data are collected in Table 1.

UV-Vis diffuse reflectance spectra were recorded over the wavelength range $\lambda = 250$–800 nm using a Cary 5G UV-Vis-NIR spectrometer Varian. MgO was used as a reference for the samples.

TPD patterns of chemisorbed H_2 were recorded with a quadrupole mass spectrometer (Dycor MA100M-Ametek) connected on-line with a micro reactor. The samples (0.50 g) were placed in a glass reactor and heated from room temperature up to 773 K at 2 K min^{-1} in a He flow of 100 ml/min and then reduced at 573 K for 1 h under H_2 flow of 100 ml min^{-1}. After reduction the samples were cooled to room temperature under atmosphere of H_2. The TPR profile was recorded upon heating the sample from 298 to 1273 K in the flow of He at 10 K min^{-1}.

Infrared spectra measurements with CO adsorption were carried out with a Nicolet Magna 750 infrared Fourier transformed spectrometer with a deuterated triglycine sulphate pyroelectric detector (DTGS-KBr) at a spectral resolution of 4 cm^{-1}. The experiments ware performed in a system “Spectra Tech” with diffuse reflectance cell and DRIFT reactor cell with ZnSe windows. Following a thermal treatment in flow of N_2 at 100 ml min^{-1}, the samples were reduced from room temperature up to 773 in H_2 (25%)/N_2 flow at 10 K min^{-1} and then maintained at 773 K for 2 h. After reduction the DRIFT cell was purged with a flow of N_2 (100 ml min^{-1}) for 20 min and then the spectra were recorded. For experiments involving analysis of ruthenium carbonyl species, the catalysts were exposed to pulses of CO in flow of N_2 for 5 min at room temperature and pressure of 160 Torr.

The energy-filtered TEM was carried out on a Carl Zeiss CEM 902 TEM machine equipped with Cataing–Henry–Ottensmeyer filter spectrometer within the

column was used. For individual zeolite particle examination, the images were obtained using zero loss energy, loss energies between 20 and 30 eV and specific elemental energies. When monochromatic inelastically scattered electrons are selected, electron spectroscopic images are formed, in which the contrast is dependent on the local energy loss spectrum and thus on the concentration fluctuations of a particular chosen element. The electron energy loss spectroscopy (EELS) was obtained at the L2, 3 edge of Ti (455 eV) and used as reference to acquire elemental maps distribution (ESI), using the three windows method [22]. Alternatively, EELS-image was obtained in the energy loss range from 390 to 476 eV, with a 6 eV slit.

2.3. Test reaction

The CO_2 reforming reaction of CH_4 was carried out in a continuous flow tube reactor at 1 atm pressure with a constant feed composition of $CH_4/CO_2/N_2$ (20/20/60) at a total flow rate of 100, 200 and 300 ml min^{-1}, with a 0.2 g of catalyst. The Ru catalysts were tested in the temperature range of 723–873 K. Some catalysts were tested at feed composition of CH_4/CO_2 of 66/33 to evaluate the thermal stability over period of 60 h. The reaction data was monitored after 15 min on stream. The rates for methane consumption, r_{CH_4}, and for carbon oxide formation, r_{CO}, for Ru supported catalysts were calculated per gram of Ru on catalyst surface under different CH_4 conversions obtained by variation of the total flow rate. Reaction products were analyzed by on-line gas chromatography, employing a combination of two GCs (Varian-3400) having a TCD detector. One chromatograph employed He and the other N_2 as carrier gas. For reaction product analysis, two columns of Porapak N and Molecular Sieve 13× were used in a series-bypass arrangement.

3. Results

3.1. XRD data

XRD patterns of Ru(Ti)/NaY and Ru(Ti)USY catalysts are shown on Fig. 1A and B, respectively. A slight decrease in the intensities of the XRD patterns of Ru/NaY and Ru/USY zeolites after submission to ion exchange with Ru is observed (Fig. 1A(a) and (b)). This can be assigned to a structural modification that would be occurred after some dealumination of the zeolite framework (Table 1).

The intensities of the XRD patterns characteristic of NaY zeolite decrease significantly when Ru/NaY is submitted to ion exchange with a solution of ATO (Fig. 1A(c)). The position of the peaks is slightly changed and the mean value of a_0 calculated from the strong diffraction peaks along 20.4, 23.7, 27.1 and 31.5° corresponding to (4 4 0), (5 3 3), (6 4 2) and (5 5 5) directions [23] decreased (from 24.65 to 24.36 for NaY and RuTiNaY, respectively) with a strong increasing of Si/Al ratio by proceeding titanium modification as seen in Table 1. Although the amount of introduced Ti in the zeolite is high, the Al content

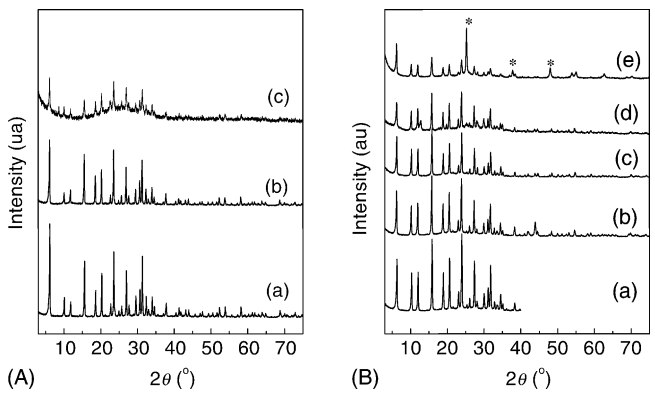

Fig. 1. XRD of Ru(Ti)/NaY (A) and Ru(Ti)/USY (B) samples. (A): (a) NaY; (b) Ru/NaY; and (c) RuTi/NaY. (B): (a) NH_4USY; (b) Ru/USY; (c) RuTi/USY; (d) Ru(2)Ti_i/USY; and (e) Ru(4)Ti_i/USY.

decreases, being supported by the higher values of Si/Al ratios of RuTi/NaY sample. A new diffuse reflectance band in the large 2θ region of 20–33° is observed, that can be connected with the presence of an amorphous material. It means a partial destruction of the zeolite structure, may be, due to a formation of larger pores caused by the strong dealumination of the zeolite framework during ion-exchange process with Ti. In addition, Ti species incorporated into zeolite does not form a separate phase from the zeolite, being seen from the XRD patterns (Fig. 1A(c)).

There is a very slight change in the intensity of XRD patterns of Ru/USY sample after submission to ion exchange with titanium (Fig. 1B(c)). The Si/Al ratio retains practically constant after introduction of Ti into Ru/zeolite (Table 1). The Si/Al ratios for USY-supported zeolite catalysts determined by XRD and chemical analysis can vary little within experimental error and it is reasonable to conclude that there is no change in the ratios. A significant decrease of the intensity of the XRD patterns of the Ru/USY zeolite after impregnation with a solution of $(NH_4)_2TiO(C_2O_4)_2{\cdot}H_2O$ is observed (Fig. 1B(d) and (e)). $RuTi_i$/USY zeolite with 4 wt.% of Ti shows diffraction peaks at 25.28, 37.80 and 48.12° (Fig. 1B(e)), which can be related to the characteristic reflections from (1 0 1), (0 0 4) and (2 0 0) planes of anatase [24], respectively. These peaks are not observed in the diffraction patterns of $RuTi_i$/USY sample with lower Ti loading (2 wt.%). May be, the amount of Ti is not enough to give clear diffraction peaks of titania. However, a change of the background of this zeolite is observed, meaning a presence of structural collapse. It can be assumed, that a substantial crystal structure of USY zeolite is still retained, although the crystallinity of the USY zeolite decreases significantly with increasing of the amount of introduced titanium.

3.2. UV-Vis spectra

Diffuse reflectance spectra of USY-supported samples and bulk TiO_2 in the region of 275–800 nm are shown in Fig. 2. An UV absorption edge at about 420 nm occurs for unsupported TiO_2 caused by $Ti^{4+} \leftarrow O^{2-}$ charge transfer. Introduction of titanium into the zeolite leads to a blue shift of the absorption band from 420 (for bulk TiO_2) to about 365 and 371 nm for RuTi/USY and $Ru(2)Ti_i$/NaY,

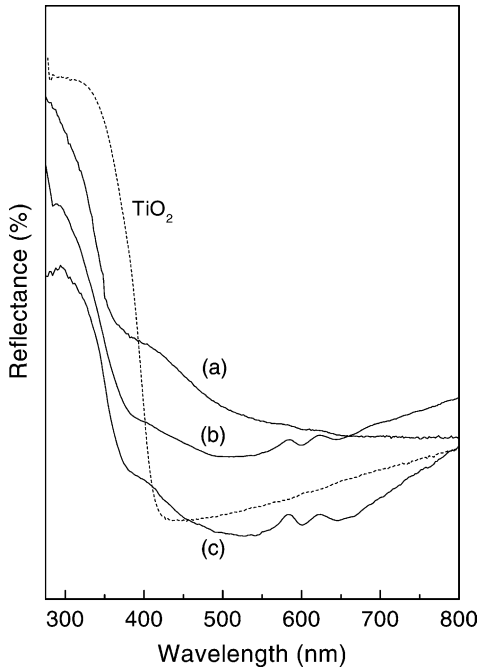

Fig. 2. UV-Vis diffuse reflectance spectra of bulk TiO_2 and zeolite-supported catalysts: (a) RuTi/USY; (b) $Ru(2)Ti_i$/USY; and (c) $Ru(4)Ti_i$/USY.

respectively (Fig. 2(a) and (b)). The mechanism that causes the blue shift of the absorption of semiconductors was usually attributed to quantum size effect [25]. Shifting of the band to lower energies (eV) suggests a decreasing of the size of TiO_2 particles [19]. A blue shift from 420 to 383 nm is observed for Ti-impregnated Ru/USY sample with the highest Ti loading (Fig. 2(c)). It suggests that the size of impregnated Ti species is higher compared to that for Ti species obtained by ion exchange. It can be concluded that the UV absorption band position depends on the amount of titanium and on the method of its introduction into the zeolite.

3.3. TPD-H_2 results

The TPD-H_2 profiles of Ru/USY and RuTi/USY samples present in Fig. 3A and B, respectively. A change in the temperature of the maximum of the main peaks is observed for the samples with and without of Ti. A strong peak at 1020 K is occurred in the spectrum of Ru/USY sample (Fig. 3A). The spectrum of

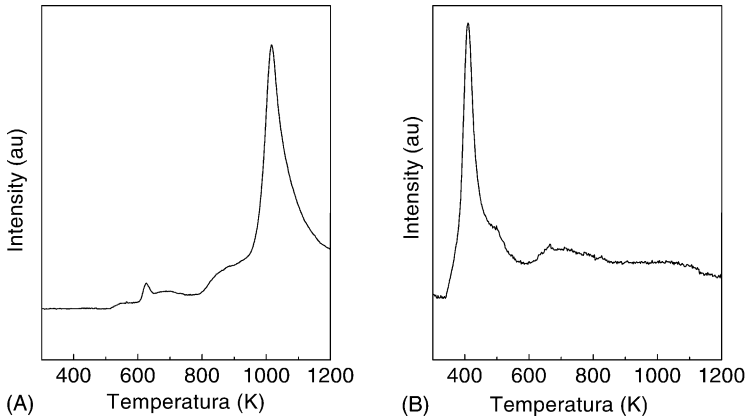

Fig. 3. TPD-H_2 patterns for Ru/USY (A) and RuTi/USY (B) samples.

Ti-exchanged Ru/USY sample shows a strong TPD peak in the lower temperature region at 410 K and small ones at about 665 and 1064 K (Fig. 3B). The main peak at 410 K can be related to desorption of H_2 from Ru particles located in the zeolite super cages [10]. However, the high temperature peak at 1020 K in the spectrum of Ru/USY zeolite (Fig. 3A) is not due to a desorption of H_2 from Ru particles, because it is difficult to reconcile such a high temperature requirement with desorption of H_2 from Ru. Similar to the observation of Lerner et al. [26] on the Pt/mordenite system, it can be supposed that the hydrogen released at the high temperature from Ru/USY after reduction at 500 K is due to a re-oxidation of very small Ru particles, most likely, isolated Ru atoms, which are located in the cavities and/or hexagonal prisms.

3.4. FTIR of CO adsorption

The infrared spectra of CO adsorbed on reduced USY-supported Ru and RuTi samples in the region 2200–1900 cm^{-1} are shown in Fig. 4. Two regions in the CO spectra are appeared: (i) high (2180–2126 cm^{-1}); and (ii) low energy region (2100–2000 cm^{-1}). Two high frequency CO bands at 2157 and 2134 cm^{-1} are observed in the spectrum of Ru/USY sample (Fig. 4(a)). The observation of such species is reported in most of the works dealing with CO adsorption on supported and reduced ruthenium catalyst. The higher frequency bands may be assigned to adsorption of CO on charged Ru^{n+} species [27,28], connected with the presence of electron-deficient Ru or the presence of Ru with different electronic structure: Ru^{2+} and/or Ru^{3+} ions. In the lower energy region a band at 2086 cm^{-1} appears as a shoulder on

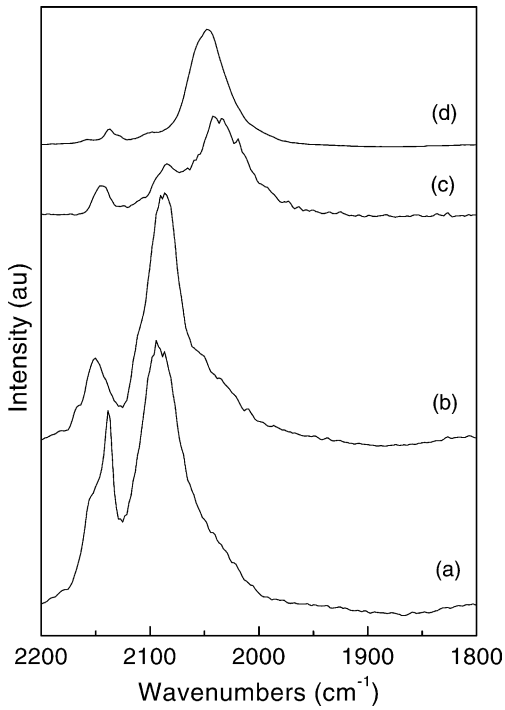

Fig. 4. FTIR of CO adsorption on Ru/USY ((a) and (b)); RuTi/USY (c); and Ru(2)Ti_i/USY (d) samples. The spectrum of Ru/USY after purged in N_2 at 373 K (b).

the strong band at 2099 cm^{-1}. A shoulder at about 2041 cm^{-1} is also detected that can be attributed to linear metal Ru°–CO carbonyls [29,30]. The intensity of the 2099 cm^{-1} band is changed after purged in He at 373 K, while the shoulder at 2041 cm^{-1} is preserved (Fig. 4(b)), meaning that the high frequency band belongs to a different species.

The main feature in the spectra of Ti-containing Ru/USY zeolites is the broad low frequency band that is centered at 2036 cm^{-1} for Ti ion-exchange sample and shifts to 2048 cm^{-1} for Ti-impregnated sample (Fig. 4(c) and (d)). This frequency shift is typical for CO adsorption on transition metal surfaces and it has been interpreted in terms of surface heterogeneity or adsorbate interactions [31]. In addition, there is a change in the shape of this band; the FWHM of the band for Ti-impregnated sample is lower. The higher frequency bands did not appear in the spectrum of reduced Ti-impregnated Ru sample, whereas the intensity of these bands is very low for Ti exchange Ru/USY zeolite. Similar observations has been reported by Brown and Gonzalez [32] after CO adsorption on silica-supported Ru catalyst submitted to reduction at 598 K for 6 h; a strong band at 2030 cm^{-1} and two weak bands at 2150 and 2080 cm^{-1}. Only one strong band at 2030 cm^{-1} has been observed after CO adsorption on reduced Ru/alumina sample with particle size greater than 90 Å [33].

3.5. Electron microscopy

Figs. 5 and 6 show TEM micrographs of Ru and RuTi/USY samples after auto-reduction in flow of He, respectively. It is clearly seen the presence of well-dispersed Ru particles of 1.5–2.5 nm inside the USY zeolite (Fig. 5). Fig. 6A is an elemental energy loss map of Ti obtained by three window method; the clear areas correspond to titanium rich domains. At the same area 43 images were acquired around the edge of titanium, using EELS-image method; the presence of that element was verified at each point of image assembly, where the spectroscopic signal is a function of variation in the intensity of entire collection of analyzed pixels. It can be seen that titanium is distributed all within the sample, including the darker regions, where due plural scattering, which is function of

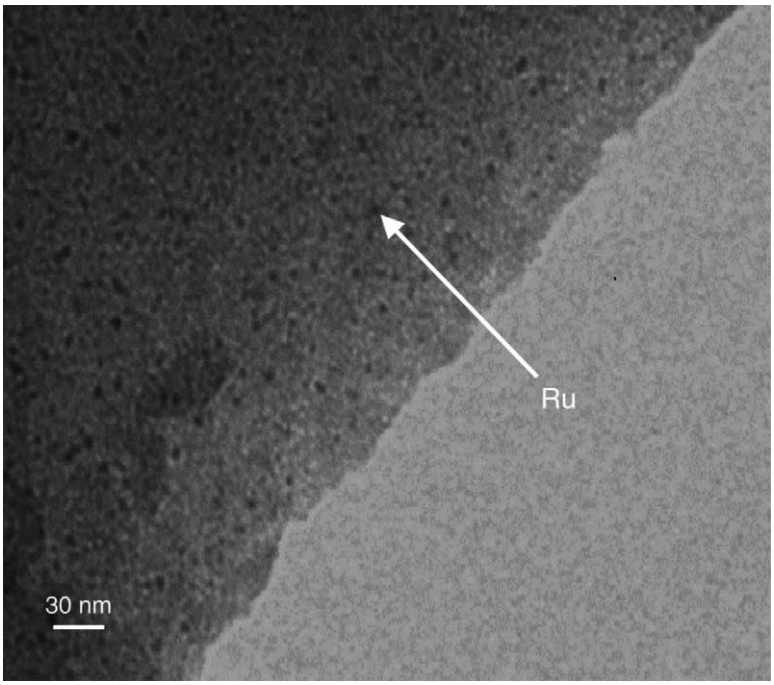

Fig. 5. Bright field image of Ru/USY sample.

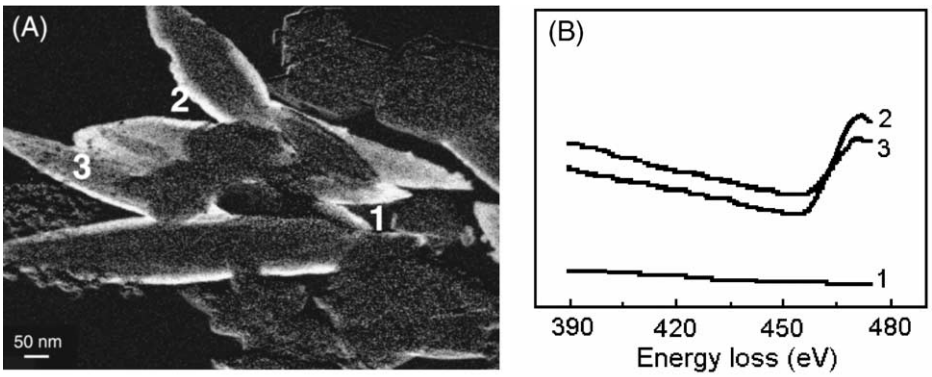

Fig. 6. Elemental spectroscopic image of Ti in RuTi/USY sample (A) and Ti spectra from EELS-image series (B).

thickness, caused a decrease in the signal. Positions 2 and 3 marked in Fig. 6A show the presence of titanium. Position 1, that is a control area without particles, does not show the presence of Ti (Fig. 6B).

3.6. Catalytic activity data

Catalytic activity data for NaY- and USY-supported Ru and RuTi catalysts in the reaction of CO_2 reforming of CH_4 at 773 and 873 K temperatures are listed in Table 2. It is seen that the conversions of CH_4 and CO_2 are influenced by: (i) the type of zeolite; (ii) method of introduced Ti species; and (iii) concentration of the metals. Ru ion-exchanged NaY zeolite exhibits higher CH_4 conversion as well as higher CO_2 conversion compared to those of Ru ion-exchanged USY zeolite (Table 2). Ti-containing catalyst supported on NaY also shows higher conversions compared to those supported on USY. This must be connected with the higher Ru loading, as well as of Ti introduced in NaY zeolite (Table 1). For Ti-impregnated Ru/USY catalysts the conversions increase with increasing of Ti loading (Table 2).

It has been shown [18] that the reaction equilibrium for the production of synthesis gas from CH_4 reforming with CO_2 (Eq. (1)) is strongly influenced by the

Table 2
Catalytic activity of the Ru and RuTi/zeolite catalysts at temperature of reaction of 773 and 873 K (flow, 100 ml min^{-1})

Sample	Temperature reaction (K)	CH_4 conversion (%)	CO_2 conversion (%)	H_2/CO	r_{CH_4} (mol g^{-1} Ru s) $\times 10^{-3}$	r_{CO} (mol g^{-1} Ru s) $\times 10^{-3}$
Ru/NaY	773	14.5	19.9	0.69	0.34	0.40
	873	32.6	35.5	0.90	0.76	0.80
RuTi/NaY	773	19.6	31.2	0.54	0.46	0.60
	873	44.2	52.6	0.83	1.05	1.15
Ru/USY	773	7.4	9.6	0.74	0.24	0.27
	873	24.5	28.6	0.85	0.78	0.84
RuTi/USY	773	15.9	22.2	0.64	0.51	0.62
	873	39.2	48.1	0.80	1.27	1.41
Ru(2)Ti_i/USY	773	13.8	19.6	0.65	0.50	0.61
	873	34.5	47.1	0.69	1.28	1.51
Ru(4)Ti_i/USY	773	15.3	19.8	0.74	0.57	0.66
	873	44.2	55.6	0.77	1.66	1.87

simultaneous occurrence of the reverse water gas shift (RWGS) reaction (Eq. (2)), in which H_2 produced via reforming reacts with CO_2 to yield H_2O and CO:

$$CH_4 + CO_2 \Leftrightarrow 2H_2 + 2CO \quad (1)$$

$$CO_2 + H_2 \Leftrightarrow CO + H_2O \quad (2)$$

According the kinetic investigations of CH_4 reforming with CO_2 some authors have shown that RWGS reaction operates very close to thermodynamic equilibrium [34,35], others have assumed [36] that the WGS reaction to be at thermodynamic equilibrium to facilitate analysis. Bradford and Vannice [18] have reported that RWGS reaction is near thermodynamic equilibrium over a wide range of temperatures.

From Table 2 it is seen that the values of CO_2 conversions for the catalysts are higher compared to those of CH_4 conversions as a consequence of the RWGS equilibrium [18]. The conversions increase with increasing of the reaction temperature. It should be expected that the H_2/CO ratios be also increased. All catalysts at 773 and 873 K show H_2/CO ratio lower than 1 (Table 1). The measured H_2/CO ratios from Table 2 showed good agreement with those calculated by Eq. (3), presented by Bradford and Vannice [9] when the reaction equilibrium is influenced by the RWGS reaction:

$$\frac{H_2}{CO} = \frac{3 - r_{CO_2}/r_{CH_4}}{1 + r_{CO_2}/r_{CH_4}} \quad (3)$$

where r_{CH_4} and r_{CO_2} are the experimental rates of CH_4 and CO_2 conversions, respectively (Table 2).

There is a strong relation between carbon dioxide conversions and the H_2/CO ratios; the H_2/CO decreases with increasing of CO_2 conversion (Table 2), confirming the strong influence of the water gas shift equilibrium. The dependence of the rate of CO formation on the partial pressures of CO and H_2 for different catalysts, plotted in Fig. 7, is approximately linear. It appears that the observed variation of catalyst activity with partial pressures for CO_2 reforming of CH_4 is due to the reverse reaction, i.e. CO hydrogenation, as was shown previously using a similar analysis [10,11]. The observed trend in r_{CO} with partial pressures of H_2 and CO shows a strong influence of the pressures over Ti-containing catalysts. However, the influence of reverse reaction is higher over Ru supported catalysts under these reaction conditions. The results indicate that significantly high space velocity must used to maintain lower conversions that decrease effluent partial pressures of H_2 and CO. This minimizes the influence of the reverse reaction during kinetic studies of CO_2 reforming of CH_4 as was shown in our previously published works [10,11].

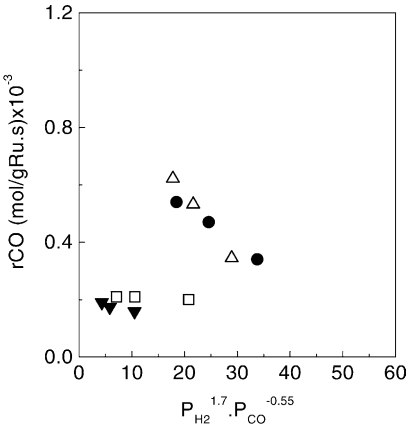

Fig. 7. Rate for carbon oxide formation as a function of the effluent partial pressures of H_2 and CO at 723 K over RuTi/USY (△); RuTi/NaY (●); Ru/USY (□); and Ru/NaY (▼).

The H_2/CO ratio is nearly unity for Ru ion-exchanged catalysts with different weight loadings of Ru. This ratio is lowered for Ti-containing catalysts, due to a strong influence of the RWGS reaction. Considering the preparation method the impregnated catalysts show lowest H_2/CO ratio and higher specific activities that increase with Ti loading.

4. Discussion

4.1. Structural properties of zeolite-supported Ru and RuTi catalysts

Change in the zeolite structure after replacement of the ions in NaY and NH_4USY by Ru and Ti is evident by comparison of the XRD patterns of the zeolites before and after ion exchange and/or impregnation process. For zeolites submitted to ion exchange with Ru less structural changes are observed compared to those submitted to Ti deposition. The changes in the structural properties of the both zeolite-supported metal catalysts account to the different pore size of these materials. The slight change in the Si/Al ratio and N_{Al}/cu (Table 1), as well as the increase of pore volume (from

0.13 to 0.24 $cm^3\,g^{-1}$ for NaY and Ru/NaY, respectively) would be result of some diffusion of Ru to the external surface of zeolite during heating in He up to 773 K, although most of the metal was inside of the zeolite framework being seen by TEM [10]. The higher Si/Al ratio determined by ICP analysis for Ti-modified Ru/NaY sample (Table 1), probably is caused by the net acidity of $(NH_4)_2TiO(C_2O_4)_2{\cdot}H_2O$ solution (pH ≅ 3), which provokes a strong dealumination of the zeolite framework. On the other hand, a negative effect of the protons within the zeolite on the size of metal particles is revealed similar for rhodium in HY and NaY zeolites during hydrothermal treatment [17,37,38]. The protons formed after auto-reduction of $[Ru(NH_3)_6]^{3+}$ complex in Ru/NaY zeolite and then connected with H_2O from aqueous solution of ATO can provoke a hydrolysis of Al–O bonds. This involves a localized destruction of the lattice and a secondary pore system is generated. The pore volume of Ru/NaY zeolite increases significantly after introduction of Ti (up to 0.63 $cm^3\,g^{-1}$), corresponding to formation of mesopores (Table 1). Filling of these pores by titanium metal species will result in easily particle agglomeration that leads to a structural collapse. The latter is supported by the significant change in the background of the XRD patterns for RuTi/NaY sample (Fig. 1).

It is surprising the increased amount of Ti for Ti-exchanged NaY sample compared to that for RuTi/USY, independently on the higher Si/Al ratio for the first one (Table 1). It should be suggest that the amount of incorporated titanium would be affected by the ion-exchange capacity of the corresponding zeolite. One of the reasons why Ti is incorporated in excess as compared with the number of Al content of RuTi/NaY zeolite is the formation of Ti–O–Si bonds during preparation procedure according the proposed mechanism by Chen et al. [24]. The authors supposed that during calcination titanyl ions (TiO^{2+}) reacted with the lattice oxygen to give TiO_2 or TiO^+, a rehydroxylation brings about acidic hydroxyls and the Al–O–Si and Ti–O–Si bonds are formed. The formation of these bonds leads to a strong structural deformation of the framework of NaY zeolite, since the amount of Ti–O–Si bonds increases with the amount of incorporated Ti. The above-mentioned authors suggested also that Ti species formed in NaY zeolite not only originated from the titanyl ion introduced by ion-exchange process, but also can be formed from the decomposition of titanyl oxalate salt which remained on the zeolite by the impregnation process, followed by calcination [24]. Therefore, it cannot be assumed that the ion-exchange capacity of NaY zeolite is higher compared to that of USY. The higher amount of introduced Ti species into Ru/NaY zeolite is due to both: (i) Ti ion exchanged; and (ii) filling of the larger pores formed after structural collapse of the zeolite with titanium species. Contrary to that, the low Ti and Ru content for Ti-exchanged Ru/USY zeolite is due to the higher Si/Al ratio, obtained after acidic Al leaching of initial USY zeolite.

TEM data for Ru/USY and RuTi/USY zeolites show that all the species present in the samples are ion exchanged and located inside the zeolite cavities. No observable TiO_2 crystalline patterns in the XRD spectra and the significant blue shift in the UV-Vis spectrum for Ti species suggest that the particle size of these species in the exchanged samples is very small. In addition, TEM data support that Ti ions, anchored within the zeolite cavities by ion-exchange method, are well-dispersed titanium oxide species. However, titanium oxide species forms a separate phase from the zeolite after impregnation of Ru/USY zeolite with solution of ATO at higher Ti content, being seen from the XRD patterns (Fig. 1B(e)). This can be connected with the pore plugging with aggregated TiO_2 crystallites, originated from the decomposition of titanyl oxalate salt during heating in flow of He up to 773 K. The average pore volume was changed from 0.27 to 0.11 $cm^3\,g^{-1}$ for Ru/USY and Ru(4)Ti_i/USY, respectively. In addition, a big fraction of large TiO_2 crystallites is accumulating on the external surface of the USY zeolite.

IR data of CO adsorption show that the local environments of ruthenium particles on each sample are quite different. The appearance of high frequency bands in reduced Ru/USY catalyst is connected with the presence of isolated, electro-deficient Ru atoms. It is well known [39] that the extent of the electron deficiency depends on the proton concentration and the size of the metal clusters in agreement with the model of metal-proton adducts $[Me_n–H_x]^{x+}$, in which the positive charge is distributed between metal and hydrogen atoms. Consequently, the electron-deficient Ru can be ascribed to electron sharing with zeolite protons from USY zeolite, which can be formed after thermal decomposition of NH_4^+ ions and/or as a co-product

of reduction of ruthenium cations with H_2. Once the metal-proton adducts were formed in Ru/USY zeolite, the reduction of Ru particles would be difficult and more electron-deficient ions will present in the framework of reduced Ru/USY zeolite. McCarthy et al. [40] have been attributed the CO FTIR band at about 2099 cm^{-1} (Fig. 4(a)) to the presence of very small metal particles and a high proton concentration in zeolite framework of Ru-exchanged NaY zeolite. From Fig. 4 it is seen that the position of the high frequency bands is sensitive to the method of preparation of zeolite-supported catalyst. The main band at 2099 cm^{-1}, as well as, another high frequency bands are not present in the IR spectra of Ti-containing samples upon reduction as a consequence of the absence of the interaction between protons and Ru metal particles. It means that auto-reduction in He up to 773 K followed by reduction at 773 K produces fully reduced ruthenium particles in RuTi samples, as well as agglomeration of the particles, being seen by the IR band at 2030–2050 cm^{-1} (Fig. 4).

It is clear that the agglomeration of Ru particles in USY zeolite is reduced when the aluminium extra framework is eliminated and the metal dispersion of the catalyst increases with increasing of Si/Al ratio (TEM, Table 1). As the zeolite is dealuminated to a greater extent, the intensity of exchangeable sites (tetrahedral Al) become lower, thus making these sites more separated within the zeolite crystallites. After ion exchange the Ru ions will be more isolated from each other and less metal sintering would be occurred. On the other hand, Ru atoms can be anchored with protons from the zeolite and/or with protons formed after auto-reduction in He in metal-proton adducts. It is known [41] that two main reasons has been considered for the suppression of hydrogen chemisorption: (i) the small size of the formed metal clusters; and (ii) the interaction of the clusters with protons of the zeolite and formation of metal-proton adducts, that leads to a change in the electronic structure (Fig. 4) of Ru clusters. This induces a lowering of the propensity of Ru particles in Ru/USY zeolite to chemisorb hydrogen during reduction in flow of H_2. The presence of mono-atomic Ru in $[Ru_n–H_x]^{x+}$ adducts could be easily re-oxidized by protons to Ru^{n+}, similar to Pt in HY and NaY zeolites [41], and the H_2 evolution will be registered at higher temperature of 1020 K.

Contrary to that, Ru atoms, which are preliminary formed in sodalite cages and/or hexagonal prisms of USY, migrate to the supercages after both, the incorporation of Ti and reduction treatment, where they agglomerated (TEM). The protons will be left behind in the small cages. Therefore the formation of $[Ru_nH]^+$ adducts will be limited in the supercages; the majority of Ru will exist as neutral Ru clusters, which have a higher propensity to chemisorb a hydrogen [17].

In is interesting to note, that the intensity of the peaks due to bridged hydroxyl groups at ca. 3740 cm^{-1} in the OH region of the IR spectra of Ru/USY samples after CO adsorption (the spectra are not shown) decreases as result of CO chemisorption on Ru. This suggests that protons in $[Ru_n{}^{\circ}–H_x]^{x+}$ adducts are partially displaced by CO.

4.2. Catalytic activity

The difference in the activity of zeolite-supported Ru only catalysts can be related to the accessible metal surface area of ruthenium particles. It has been shown [10,11] that the influence of zeolite as support was limited to affect the metal dispersion during the course of the catalyst preparation and stabilization of the metal surface area under reaction conditions, which is responsible for catalyst activity, similar to the inert SiO_2 support [16].

The more active Ru/NaY catalyst compared to Ru/USY can be related to the higher Ru loading, as well as to the difference in the dispersion of Ru species. As was supposed above the Ru species located in supper cages of NaY would be easily reduced during preliminary reduction and under reaction conditions. TEM micrographs show the presence of small Ru particles of 1–2 nm, consequently well-dispersed metal in USY. This causes a easily formation of metal-proton adducts in the cavities of Ru/USY zeolite (TPD, FTIR), which inhibits the dissociative adsorption of methane on Ru particles, like to the inhibition of dissociative chemisorption of H_2 [42] causing the decrease in CH_4 and CO_2 conversions.

Considering the presence of Ti the order of activity compared by specific activities (r_{CH_4} or r_{CO}) for zeolite-supported catalysts decreases in the following order: $Ru(4)Ti_i$/USY > RuTi/USY > $Ru(2)Ti_i$/USY > RuTi/NaY > Ru/NaY > Ru/USY (Table 2). It can be concluded that all Ti-containing samples

show higher catalytic activity compared to those without Ti as it is more evident for catalysts supported on USY zeoilite. The catalytic activity increases with increasing of Ti content. The influence of RWGS reaction is greater for catalysts containing Ti.

It is evident that the rate data (Table 2) reflect the participation of titania in the catalytic cycle, although the reforming of CH_4 with CO_2 has been reported to be structure sensitive over titania-supported noble metals for dispersion above 25% [8,13]. The difference in the activity may be related to the activation of the CH_4 and CO_2 dissociation, which requires electron donation from the surface. The activation of CH_4 on the metal surface is the rate-limiting during CO_2 reforming of CH_4, as reported previously, which involves the dependence of catalytic activity on %d-character of metal [7]. It has been reported that the introduction of a strong metal-support interaction (SMSI) effect into TiO_2-supported metal catalysts correlated with the increasing of electron density in the metal crystallites [8,13] and formation of active interfacial Ru–$Ti^{n+}O_x$ species. DRIFTS results [9,43] have considered that CH_4 dissociation to CH_x and CH_xO species, as well as CO_2 dissociation to anionic CO_2-precursor [44] can be accelerated on metal-support interfacial region because of creation of new active sites, like metal$-Ti^{n+}$ or metal–$Ti^{n+}-O^{m-}$ sites. The electron effects may become significant when the supported metal Ru particles are well dispersed on the zeolite support as in the case of Ni/TiO_2 [7], where Ni was speared in thin rafts on the support surface. Therefore, the specific activity of Ti-containing Ru/zeolite catalysts are higher than for supported Ru catalysts (Table 2) because of the creation of new active sites in metal-support interfacial region, which can accelerate the formation of CH_xO decomposition, precursor for CO formation.

It cannot be excluded the acidic nature of these catalysts. According the literature [45] the higher value of Si/Al ratio for NaY-supported RuTi catalyst compared to those for dealuminated USY catalysts means that a significant number of acidic aluminium is retained in the zeolite after dealumination. This leads to a generation of acid sites that could promote the hydrogenation of carbon oxide [46]. However, the higher rate for CO formation for RuTi/NaY catalyst (Table 2) suggests that the influence of the acidity is minimized in the reaction of CO_2 reforming of CH_4. In the same time, the reaction on zeolite-supported Ru catalysts would be catalyzed by "the electron deficient" of $[Ru_nH]^{n+}$ adducts. Therefore, the decrease of CO formation can be related to a hydrogenation of CO similar to our previous observations [10].

The Ru and TiRu supported catalysts showed high stability in the activity under reaction conditions during 60 h. Different opinions have been proposed about the high stability of zeolite-supported noble metals [16,47]. Ones authors connect the high thermal stability with the high dispersion of metal particles. However, Bhat and Sachtler [17] have shown that the high thermal stability of Rh/NaY zeolite in CO_2 reforming of CH_4 was related to large Rh particles of 40 Å, which are formed in the initial stage of the catalytic operation: ones they are formed no further agglomeration take place. On the other hand, it has been shown [7,8] that TiO_2-supported group VIII metals exhibit suppressed carbon formation during CO_2 reforming of CH_4 due the decoration of metal particle surfaces by TiO_x species which destroy large ensembles of metal atoms that serve as active sites for carbon formation.

5. Conclusions

The relative amount of electron-deficient Ru atoms in Ru exchanged USY zeolite is higher compared to that of Ti-containing Ru/USY zeolite, due to the presence of metal-proton adducts.

Introduction of titanium into Ru/NaY zeolite by ion exchange leads to a significant structural collapse of the zeolite framework. Contrary to that, TEM data showed that Ti incorporated into Ru/USY by ion exchange is well distributed within the zeolite cavities.

The specific activity related to formation of CO increases with increasing of Ti content caused by the creation of new active sites at metal-support interfacial region, which can accelerate the formation of CH_xO decomposition, precursor for CO formation. On the other hand, the influence of reverse of water gas shift reaction on the activity is higher for Ti-containing catalysts. The reforming reaction on zeolite-supported Ru catalysts is mainly catalyzed by the presence of metal-proton adducts clusters, that causes the hydrogenation of CO.

Acknowledgements

The authors are gratefully acknowledged financial support of Fundacão para o Amparo a Pesquisa do Estado de São Paulo (FAPESP), Financiadora de Estudos e Projetos (FINEP), Conselho Nacional de Desenvolvimento Cientifico e Tecnologico (CNPq) and Petrobras.

References

[1] J.R. Rostrup-Nielsen, J.H. Bak Hansen, J. Catal. 144 (1993) 38.
[2] A.M. Gadalla, M.E. Sommer, Chem. Eng. Sci. 44 (1989) 2825.
[3] M. Levy, R. Levitan, H. Rosin, R. Rubin, Solar Energy 50 (1993) 179.
[4] J.R. Rostrup-Nielsen, J.-H. Bak Hansen, L.U. Aparicio, J. Jpn. Petr. Inst. 40 (1997) 366.
[5] J.T. Richardson, S.A. Paripatyadar, Appl. Catal. 61 (1990) 29.
[6] P.D.F. Vernon, M.L.H. Green, A.K. Cheetham, A.T. Ashcroft, Catal. Today 13 (1992) 417.
[7] M.C.J. Bradford, M.A. Vannice, Appl. Catal. A: Gen. 142 (1996) 73.
[8] Z. Zhang, V.A. Tsipouriari, A.M. Efstathiou, X.E. Verykios, J. Catal. 158 (1996) 51.
[9] M.C.J. Bradford, M.A. Vannice, Catal. Today 50 (1999) 87.
[10] U.L. Portugal, C.M.P. Marques, E.C.C. Araujo, E.V. Morales, M.V. Giotto, J.M.C. Bueno, Appl. Catal. A: Gen. 193 (2000) 173.
[11] U.L. Portugal, A.C.S.F. Santos, S. Damyanova, C.M.P. Marques, J.M.C. Bueno, J. Mol. Catal. A: Chem. 184 (2002) 311.
[12] M.C.J. Bradford, M.A. Vannice, J. Catal. 183 (1999) 69.
[13] M.F. Mark, W.F. Maier, J. Catal. 164 (1996) 122.
[14] J.B. Claridge, M.L.H. Green, S.C. Tsang, Catal. Today 12 (1994) 455.
[15] L. Basini, D. Sanfilippo, J. Catal. 157 (1995) 162.
[16] P. Ferreira-Aparicio, I. Rodriguez-Ramos, J.A. Anderson, A. Guerrero-Ruiz, Appl. Catal. A: Gen. 202 (2000) 183.
[17] R.N. Bhat, W.M.H. Sachtler, Appl. Catal. A: Gen. 150 (1997) 279.
[18] M.C.J. Bradford, M.A. Vannice, Catal. Rev.-Sci. Eng. 41 (1999) 1.
[19] X.S. Liu, K.K. Iiu, J.K. Thomas, Chem. Phys. Lett. 195 (1992) 163.
[20] X.S. Liu, K.K. Iiu, J.K. Thomas, J. Chem. Soc., Faraday Trans. 89 (1993) 1861.
[21] L.B. McCuskar, C. Baerlocher, Stud. Surf. Sci. Catal. 147 (2001) 37.
[22] C. Jeanguillaume, C. Colliex, Ultramicroscopy 28 (1989) 252.
[23] G.T. Kerr, Zeolites 9 (1989) 351.
[24] H. Chen, A. Matsumoto, N. Nishimiya, K. Tsutsumi, Colloids Surf. A: Phys. Eng. Aspects 157 (1999) 295.
[25] I.R. Beattie, V. Faecett, J. Chem. Soc. A (1967) 1583.
[26] B.A. Lerner, B.T. Carvill, W.M.H. Sachtler, J. Mol. Catal. 77 (1992) 99.
[27] G.H. Yokomizo, C. Louis, A.T. Bell, J. Catal. 120 (1989) 1.
[28] J.A. de los Reyes, M. Vrinat, M. Breysse, F. Mauge, J.-C. Lavalley, Catal. Lett. 13 (1992) 213.
[29] F.M. Hoffmann, M.D. Weisel, Surf. Sci. 269/270 (1992) 495.
[30] K. Hadjiivanov, J.-C. Lavalley, J. Lamotte, F. Mauge, J. Saint-Just, M. Che, J. Catal. 176 (1998) 415.
[31] L.H. Little, Infrared Spectra of Adsorbed Species, Academic Press, New York, 1966, p. 200.
[32] M.F. Brown, R.D. Gonzalez, J. Phys. Chem. 80 (1976) 1731.
[33] R.A.D. Betta, J. Phys. Chem. 79 (1975) 2519.
[34] O. Takayasu, N. Hongo, I. Matsuura, Stud. Surf. Sci. Catal. 77 (1993) 305.
[35] H.M. Swaan, V.C.H. Kroll, G.A. Martin, C. Mirodatos, Catal. Today 21 (1994) 571.
[36] J.R. Rostrup-Nielsen, in: J.R. Anderson, M. Boudart (Eds.), Catalysis: Science and Technology, Springer, Berlin, 1984, p. 1.
[37] T.H. Flesch, B.L. Meyers, G.J. Ray, J.B. Hall, C.L. Marshall, J. Catal. 99 (1986) 117.
[38] Q.L. Wang, G. Giannetto, M. Torrealba, G. Perot, C. Kappenstein, M. Guisnet, J. Catal. 130 (1991) 459.
[39] D.C. Tomczak, G.D. Schunemann, H. Trevino, W.M.H. Sachtler, Microporous Mater. 5 (1996) 263.
[40] T.J. McCarthy, C.M.P. Marques, H. Trevino, W.M.H. Sachtler, Catal. Lett. 43 (1997) 11.
[41] V.L. Zholobenko, G.D. Lei, B.T. Carvill, B.A. Lerner, W.M.H. Sachtler, Chem. Soc., Faraday Trans. 90 (1994) 233.
[42] L. Xu, Z. Zhang, W.M.H. Sachtler, J. Chem. Soc., Faraday Trans. 88 (1992) 2291.
[43] W. Fancheng, W. Huilin, K.R. Tsai, W. Shuiju, X. Fuchun, Catal. Lett. 12 (1992) 319.
[44] F. Solymosi, J. Mol. Catal. 65 (1991) 337.
[45] J.J. DeCanio, J.R. Sohn, P.O. Fritz, J.H. Lunsford, J. Catal. 101 (1986) 132.
[46] J.C.S. Wu, R. Oukaci, J.G. Goodwin, J. Catal. 142 (1993) 531.
[47] J. Nakamura, K. Aikawa, K. Sato, T. Uchijima, Stud. Surf. Sci. Catal. 90 (1993) 95.